SCIENTIFIC REPORTS

OPEN

SUBJECT AREAS:
IMPLANTS
MATERIALS SCIENCE
BIOMATERIALS
BIOMEDICAL MATERIALS

Received
17 April 2013

Accepted
18 July 2013

Published
6 August 2013

Correspondence and requests for materials should be addressed to H.-K.S. (drstone@kist.re.kr)

* These authors contributed equally to this work.

Biodegradability engineering of biodegradable Mg alloys: Tailoring the electrochemical properties and microstructure of constituent phases

Pil-Ryung Cha[1]*, Hyung-Seop Han[2]*, Gui-Fu Yang[2], Yu-Chan Kim[2], Ki-Ha Hong[3], Seung-Cheol Lee[4], Jae-Young Jung[5], Jae-Pyeong Ahn[5], Young-Yul Kim[6], Sung-Youn Cho[7], Ji Young Byun[8], Kang-Sik Lee[9], Seok-Jo Yang[10] & Hyun-Kwang Seok[2]

[1]School of Advanced Materials Engineering, Kookmin University, Seoul 136-702, South Korea, [2]Center for Biomaterials, Korea Institute of Science & Technology, Seoul 136-650, South Korea, [3]Department of Materials Science and Engineering, Hanbat National University, Daejeon, 305-719, South Korea, [4]Electronic Materials Research Center, Korea Institute of Science & Technology, Seoul 136-650, South Korea, [5]Advanced Analysis Center, Korea Institute of Science & Technology, Seoul 136-650, South Korea, [6]Department of Orthopedics, St. Mary's Hospital, The Catholic University of Korea, Daejeon 301-723, South Korea, [7]R&D Center, U&I Corporation, Uijongbu 480-050, South Korea, [8]Center for Materials Architecturing, Korea Institute of Science and Technology, Seoul 136-650, Republic of Korea, [9]Department of Orthopedic Surgery, Asan Medical Center, Seoul 138-736, Korea, [10]Department of Mechatronics Engineering, Chungnam National University, Daejeon 305-764, South Korea.

Crystalline Mg-based alloys with a distinct reduction in hydrogen evolution were prepared through both electrochemical and microstructural engineering of the constituent phases. The addition of Zn to Mg-Ca alloy modified the corrosion potentials of two constituent phases (Mg + Mg_2Ca), which prevented the formation of a galvanic circuit and achieved a comparable corrosion rate to high purity Mg. Furthermore, effective grain refinement induced by the extrusion allowed the achievement of much lower corrosion rate than high purity Mg. Animal studies confirmed the large reduction in hydrogen evolution and revealed good tissue compatibility with increased bone deposition around the newly developed Mg alloy implants. Thus, high strength Mg-Ca-Zn alloys with medically acceptable corrosion rate were developed and showed great potential for use in a new generation of biodegradable implants.

Owing to their high strength, ductility, and good corrosion resistance, metallic materials such as stainless steels, titanium alloys, and cobalt-based alloys represent an important class of materials in hard tissue replacement. These materials are used as load-bearing implants for the repair or replacement of diseased or damaged tissues. These metallic materials are essentially neutral *in vivo* and remain inside the body after implantation as permanent fixtures, which must be removed by a second surgical procedure after the tissue heals sufficiently[1]. Additional surgery increases costs to the health care system and causes additional stress to the patient. Thus, a new domain of research in metallic implants focuses on biodegradable implants that can dissolve in the biological environment after a certain length of functional use. When applied as a biodegradable implant material, magnesium provides both biocompatibility and suitable mechanical properties.

Large amounts of Mg^{2+} are present in the human body. These ions are involved in many metabolic reactions and biological mechanisms, and excess Mg^{2+} is easily excreted via urine[2]. When compared to currently used implant materials, magnesium and magnesium-based alloys have a higher yield strength and a lower elastic modulus of about 45 GPa, which is close to that of natural bone (10–40 GPa). These characteristics provide magnesium-based alloys with the potential to avoid stress-shielding effects[3–5]. Moreover, owing to its functional roles and presence in bone tissue, magnesium may actually have stimulatory effects on the growth of new bone tissue[6–10]. Thus, it is suggested that magnesium and its alloys can be applied as lightweight, degradable, load-bearing orthopedic implants that would remain in the body and maintain mechanical integrity over a time scale of 12–24 weeks while the bone tissue heals, eventually being replaced by natural tissue[11,12]. Previous *in vivo* studies have shown that magnesium could be suitable as a degradable biomaterial for use in medical implants[13,14].

However, some challenges prevent the practical use of biodegradable magnesium alloys. For example, commercial pure magnesium[15] and magnesium alloys can corrode too quickly at physiological pH (7.4–7.6) and under the high chloride conditions of the physiological environment. Rapid corrosion leads to the production of hydrogen gas in the corrosion process at a rate that is too fast for the host tissue to handle. Furthermore, such corrosion causes loosening of the mechanical integrity before the tissue can sufficiently heal[16–20]. Moreover, a much higher inherent strength of any developed alloys will be required because their strength would deteriorate gradually during the corrosion/degradation process[21]. Zhang *et al*[21]. reported that the bending strength of Mg-Zn alloy decreased rapidly during the initial corrosion stage, from about 625 MPa to 390 MPa with an approximately 6% loss of weight.

Zberg *et al*[22]. recently circumvented the above problems by using ternary Mg-Zn-Ca alloys in the form of bulk metallic glasses (BMGs). In their *in vitro* and *in vivo* degradation tests, these amorphous alloys showed tissue compatibility equivalent to that of their crystalline counterparts without clinically observable hydrogen production. Despite this, metallic glasses are brittle and particles can be released through wear processes, which might lead to antibody responses or inflammatory cascades, thereby reducing the overall biocompatibility[23–25]. Moreover, even though good cell viability has been reported in a cytotoxicity test[26], the high content of Zn in biodegradable Mg-Zn-Ca BMGs may be harmful to the human body[27,28] (the results of a cytotoxicity test performed at high Zn concentration are presented in the Supplementary Information). The sample dimension available for the formation of BMGs is also relatively small (of the order of several millimeters) when compared to their crystalline counterparts, which imposes a constraint on the application of Mg-Zn-Ca BMGs as biodegradable implants.

There have been several studies that considered crystalline Mg-Zn-Ca alloys as biodegradable implant materials[29–31]. However, they only reported limited phenomenological analyses, which showed that the macroscopic corrosion potential averaged over all constituent phases shifted to a more inert direction or that the ternary intermetallic compounds might be related to the increase of corrosion resistance. They could not find the optimal compositions of Mg-Zn-Ca alloys for clinical applications and failed to present any Mg based alloys with clinical significance. In this study, we developed new magnesium-based crystalline biomaterials with good mechanical properties and medically acceptable corrosion rate, which was achieved by tailoring the electrochemical properties and microstructure of constituent phases.

Table 1 | Actual compositions of the cast Mg-Ca-Zn alloys analyzed by ICP method

Alloys	Ca (wt%)	Zn (wt%)	Mg (wt%)
Pure Mg	0	0	99.98 (Fe: 14 ppm)
Mg-5 wt%Ca	4.65	0	Bal.
Mg-5 wt%Ca-0.5 wt%Zn	4.62	0.50	Bal.
Mg-5 wt%Ca-1.0 wt%Zn	4.72	0.76	Bal.
Mg-5 wt%Ca-1.5 wt%Zn	4.51	1.63	Bal.
Mg-5 wt%Ca-3.0 wt%Zn	4.56	3.00	Bal.
Mg-5 wt%Ca-5.0 wt%Zn	4.65	4.12	Bal.

Results

Commercially available pure Mg (99.98%) ingots, Ca (99.99%) metal grains, and Zn (99.99%) metal grains were used to prepare Mg-Ca and Mg-Ca-Zn alloys in a vacuum furnace. The atmosphere of the furnace was purged to 5×10^{-2} torr before high purity argon gas was applied (99.999%). The melting temperature was 750°C, and the melt was cast into a STS430 steel mold. The shape of each casting sample was a cylinder with a diameter of 50 mm and a height of 70 mm. The chemical compositions of the alloys (Table 1) were analyzed by the inductively coupled plasma (ICP) method. Mechanical extrusion was adopted for the microstructural tailoring. To accomplish this, the as-cast ingots were preheated to ~ 350°C and then extruded into rods with an extrusion ratio of 25 : 1, after which the samples were cooled in air.

As shown in Fig. 1a, a hydrogen-evolution test revealed that increasing the Zn content generated a significant change in behavior. Specifically, Mg-5 wt%Ca and Mg-5 wt%Ca-0.5 wt%Zn alloys featured strong gas evolution during degradation in Hank's solution (Methods), whereas increasing the Zn content to more than 1 wt% induced a remarkable reduction in the amount of hydrogen evolved, with the best corrosion resistance being observed at 1.5–3 wt%. Figure 1b–f shows the scanning electron microscopy (SEM) images

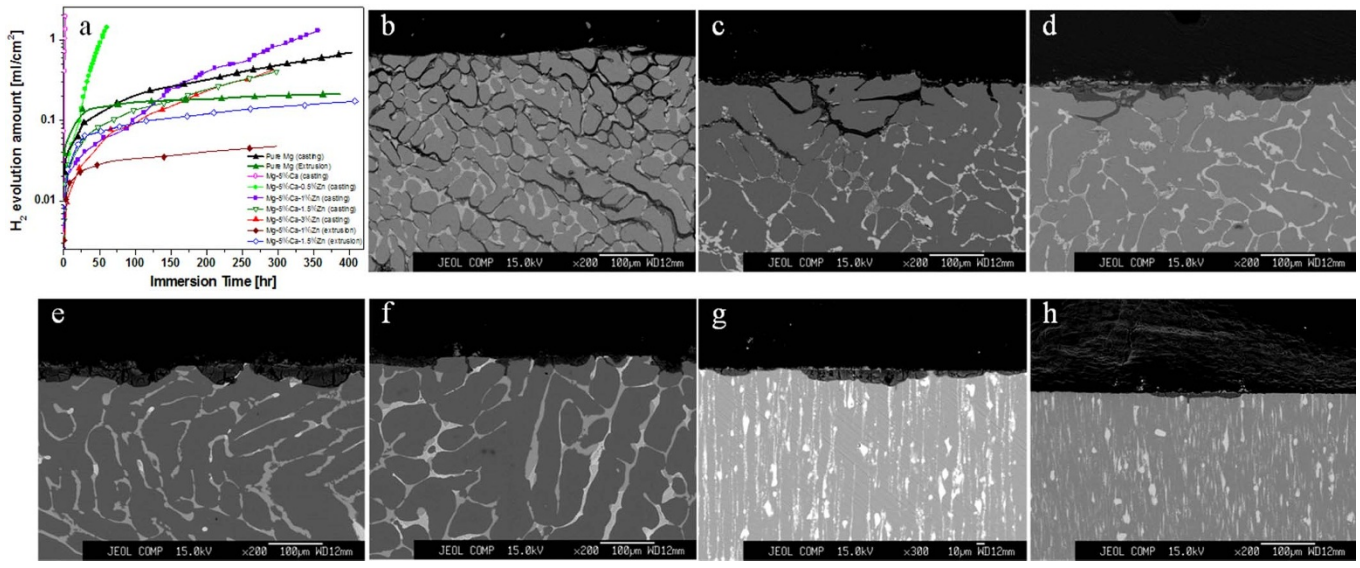

Figure 1 | Corrosion and corrosion microstructure measurements of crystalline Mg-Ca-Zn alloys. (a). Hydrogen-evolution measurements showing a distinct drop in response to the addition of Zn and by mechanical extrusion. (b–f). SEM images of Mg-5 wt%Ca-*x*wt%Zn alloy samples ($x = 0, 0.5, 1.0, 1.5, 3.0$) after the immersion test in Hank's solution. (g, h). SEM images of extruded Mg-5 wt%Ca-*x*wt%Zn alloy samples ($x = 0.5, 1.0$) after the immersion test in Hank's solution.

of Mg-5 wt%Ca-*x*wt%Zn alloy samples ($x = 0, 0.5, 1, 1.5, 3$) after the immersion test in Hank's solution. As shown in Fig. 1a, severe corrosion of the Mg-5 wt%Ca alloy occurred immediately upon immersion into Hank's solution.

The microstructure of the Mg-5 wt%Ca binary alloy is composed of a primary Mg phase and an eutectic phase, which is a lamella structure composed of Mg and Mg_2Ca phases (for the microstructures of as-cast Mg-Ca-Zn alloys, see Supplementary Information). A galvanic circuit forms when the alloy is immersed into Hank's solution owing to differences in the electro-chemical potentials of the Mg and Mg_2Ca phases. This galvanic circuit leads to swift and selective corrosion of the Mg_2Ca phase. The corroded microstructure shown in Fig. 1b demonstrates this corrosion mechanism. This type of non-uniform corrosion can result in disintegration of the alloy or deterioration of its mechanical strength during the corrosion period.

As shown in Fig. 1c, the selective corrosion of the Mg_2Ca phase caused by formation of the galvanic circuit was remarkably suppressed by the addition of a small amount of Zn. The addition of 0.5 wt% Zn modified the microstructure significantly. Specifically, the microstructure composed of primary Mg and eutectic phases changed to a mixture of primary Mg and Mg_2Ca (not lamella structure) with dissolved Zn. Mg_2Ca phases were disconnected at some places, whereas all eutectic structures in the Mg-Ca binary alloy were connected (for the modified microstructure, *see* Supplementary Information). Owing to the disconnected Mg_2Ca distribution and dissolved Zn, the selective corrosion of the Mg_2Ca phase was remarkably reduced.

When the Zn content increased to more than 0.5 wt% (see Fig. 1 d, e, f), almost no corrosion occurred during the $\sim$ 300 hours immersion test and the corrosion rates were comparable or lower than that of high purity Mg. This is the first reported observation of multi-phase Mg alloy with comparable corrosion resistance to that of high purity Mg. It is interesting to note that the Mg-Ca-Zn alloys did not experience pitting corrosion, which is a typical corrosion mode of Mg alloys. Rather, uniform and flat corrosion was observed, which implies that the alloys are free from the abrupt disintegration of the alloys and deterioration of mechanical strength during the corrosion/degradation process. The microstructures (Fig. S1 c, d, and e in Supplementary Information) of as-cast Mg-Ca-Zn alloys with more than 1 wt% Zn did not differ greatly from that of the alloy with 0.5 wt% Zn, except for the white contrast phases connected by the Mg_2Ca phases. X-ray diffraction analysis and wavelength dispersive spectroscopy (WDS) map analysis revealed that the white contrast phase was $Mg_6Ca_2Zn_3$ intermetallic compound (*see* Fig. S2 and the text in Supplementary Information for its role in the corrosion). The volume fraction of this intermetallic compound increased as the Zn content increased. However, the corroded SEM images (Fig. 1d, e, f) demonstrated that, rather than the $Mg_6Ca_2Zn_3$ intermetallic compound blocking the corrosion, the Mg_2Ca phase with dissolved Zn was not corrosive.

As shown in Fig. 1a, the effect of extrusion on the corrosion rate was significant. The corrosion rate of extruded Mg-5 wt%Ca-1 wt%Zn alloy was much lower than that of high purity Mg, which was also confirmed by weight loss measurements (*see* Supplementary Information). Figure 1g and h shows the corroded microstructures of the extruded Mg-5 wt%Ca-0.5 wt%Zn and Mg-5 wt%Ca-1 wt%Zn alloys after being subjected to the immersion test for 299 hours and 408 hours, respectively. Despite these long immersion times, a flat corrosion surface persisted after a slight initial corrosion. There are various studies reporting that the corrosion rate of the Mg decreases with decreasing grain size[32]. The average grain size of the pure Mg was refined to $\sim$ 25 μm by the extrusion whereas that of Mg-5 wt%Ca-1 wt%Zn alloy reduced to $\sim$ 10 μm. Effective grain refinement of the ternary alloy was induced by the particle pinning effect of the second phase and caused larger drop of its corrosion rate compared to high purity Mg.

Figure 2 shows the SEM and the corresponding WDS images taken to investigate the distribution of the dissolved Zn. Non-uniform distribution of Zn was observed in the Mg ternary alloys with $\geq$ 0.5 wt% Zn (Fig. 2b, c, d), which indicates that the dissolved Zn content is out of and within the solubility limit in the primary Mg and Mg_2Ca, respectively. In the SEM images shown in Fig. 2b, c, and d, dark gray indicates primary Mg and white reflects Mg_2Ca phase. Figure 2e shows the relationship between the biodegradation rate of the Mg-Ca-Zn alloys and the Zn concentration inside the Mg_2Ca phase obtained from WDS analysis. Obvious inverse proportionality was observed, which implies that the addition of Zn to Mg_2Ca prevents non-uniform corrosion by the formation of the galvanic circuit, that is, the addition of Zn to Mg_2Ca increases the corrosion potential of the Mg_2Ca phase. This is also supported by measurements of the open-circuit potential (OCP) of the immersed alloys.

As shown in Fig. 2f, the pure Mg is nobler (OCP versus standard hydrogen electrode (SHE) ≈ -1.58 V) than Mg_2Ca (OCP versus SHE ≈ -1.87 V), which demonstrates the non-uniform and rapid corrosion along Mg_2Ca by the formation of the galvanic circuit. However, the addition of Zn to Mg_2Ca pushed the OCP of Mg_2Ca up to that of the pure Mg, which prevented selective corrosion along the Mg_2Ca and induced the uniform corrosion seen in Fig. 1d, e, and f. The change in the work function of Mg_2Ca with Zn contents was investigated by using the first principle calculation to qualitatively understand the OCP increase of Mg_2Ca with Zn contents (*see* Methods and Supplementary Information). It has been reported that the corrosion potentials of metals are proportional to their work functions[33] though they are a mixed potential and a function of various factors such as chemicals in Hank's solution, complexes of positive ions and so on. Figure 2g shows the variation of the work function with Zn contents for the (0001) surface of Mg_2Ca with lowest surface energy. The inset shows the atomic configuration of the (0001) surface. The work function of Mg_2Ca in the most stable (0001) surface is 3.16 eV that is lower than that of pure Mg, say, 3.7 eV. This is consistent with OCP measurement where pure Mg has higher OCP than Mg_2Ca. The results also imply that the Zn atoms on the Mg_2Ca surface induce the increase of its work function, which is consistent with the OCP increase of Mg_2Ca with Zn concentration.

Animal experiments were performed in the dorsal abdominal region of eight adult male Sprague-Dawley rats to evaluate hydrogen evolution *in vivo*. Extruded Mg-5 wt%Ca and cast and extruded Mg-5 wt%Ca-1 wt%Zn plates, together with a reference Mg-5 wt%Ca cast alloy, were implanted in the rats and analyzed after 1, 2, 4, 8 and 12 weeks, respectively. Figure 3 shows the hydrogen evolution of Mg-Ca-Zn and Mg-Ca implants 12 weeks post-implantation. Rats implanted with cast and extruded Mg-Ca and cast Mg-Ca-Zn plates showed clinically and radiographically visible gas bubbles (Fig. 3 a, b and c). The gas bubbles were formed within the first week after surgery and persisted for the entire 12 week period. Rats implanted with extruded Mg-Ca-Zn plates did not show any visible gas bubbles clinically or radiographically (Fig. 3 d). Accordingly, there were no adverse effects caused by the gas bubbles.

The result from series of extensive animal model study has assured the possibility of developed Mg-5 wt%Ca-1 wt%Zn extruded alloy as next generation of biodegradable orthopedic material. Histologic analysis (Fig. 4 a) of extruded Mg-5 wt%Ca-1 wt%Zn alloy bone screw implanted on femoral condyle of New Zealand white rabbit for 24 weeks demonstrated new bone formation and bone remodeling without notable bubble formation and foreign body response around the implanted sample. An abundance of new bone depositions around the degraded bone screw was observed and magnified image (Fig. 4 b) of the implantation site clearly displays the active bone remodeling around the degraded implant sample. Further histomorphometric analysis of the slide confirmed a slight increase in the percentage of new bone with time, while the percentage of

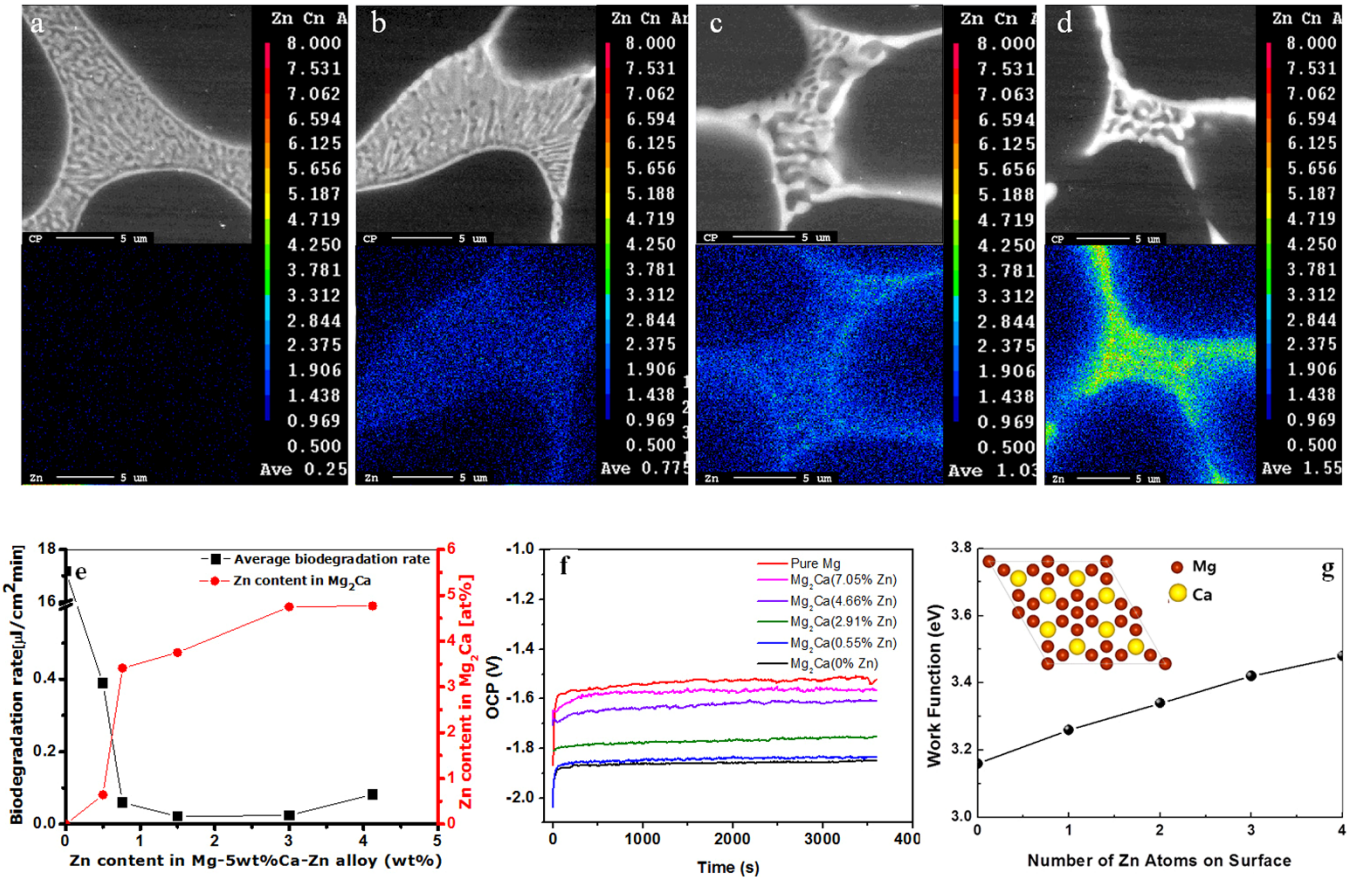

Figure 2 | (a–d). SEM and the corresponding WDS images showing the distribution of dissolved Zn in Mg-5 wt%Ca-*x*wt%Zn alloys ($x = 0, 0.5, 1.0$, and 1.5 from the left). (e). Relationship between the biodegradation rate of Mg-Ca-Zn alloys and the Zn concentration inside Mg_2Ca obtained from WDS analysis. (f). Measurement of the open-circuit potential (OCP) of the immersed Mg_2Ca alloys with various Zn concentrations. (g). Variation of the work function with Zn contents in the (0001) surface of Mg_2Ca (**Inset.** Atomic configuration of the (0001) surface where red spheres represents Mg atom and gold spheres represent Ca atom).

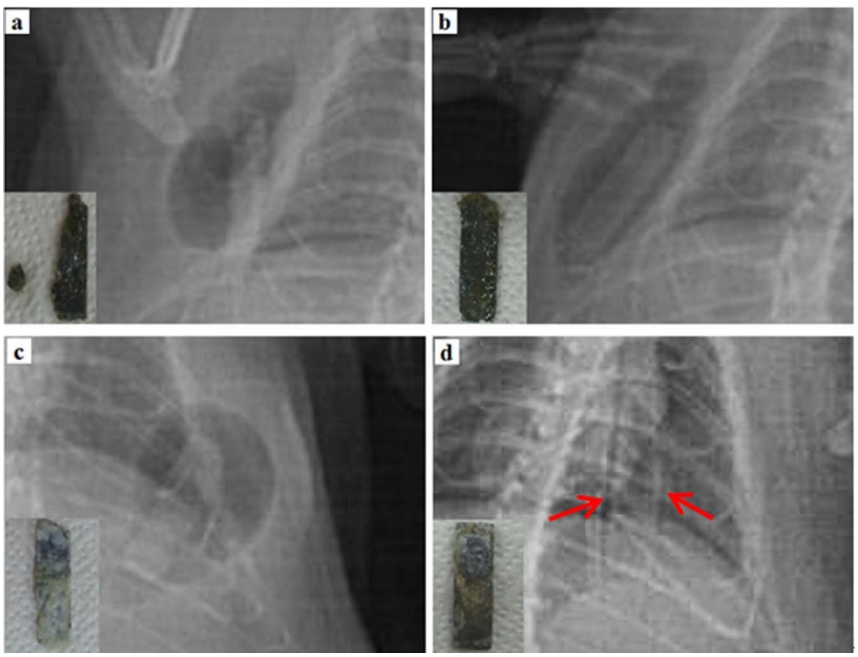

Figure 3 | **X-ray images of hydrogen bubble pockets at 12 weeks after the implantation of Mg-Ca-Zn and Mg-Ca alloy samples into the dorsal abdominal region of eight adult male Sprague–Dawley rats.** (a). Cast Mg-5 wt%Ca. (b). Extruded Mg-5 wt%Ca. (c). Cast Mg-5 wt%Ca-1 wt%Zn (d). Extruded Mg-5 wt%Ca-1 wt%Zn. **Insets:** The corresponding corroded implants removed from the rats at 12 weeks after implantation.

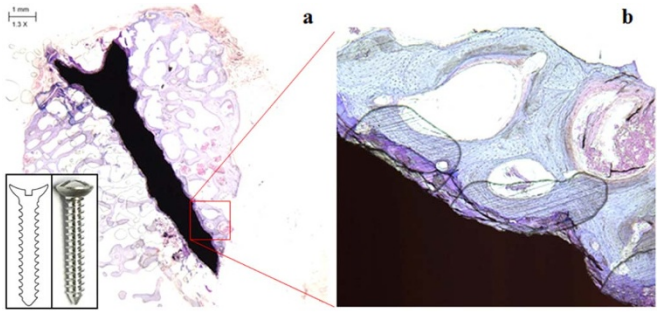

Figure 4 | Histological analysis of extruded Mg-5 wt%Ca-1 wt%Zn alloy bone screw in femoral condyle of New Zealand white rabbit using Toludine blue staining at 24 weeks after operation. (a). 3 × magnification. (b). 10 × magnification. **Insets:** The cross sectional diagram (left) and finalized sample (right) of Mg-5 wt%Ca-1 wt%Zn alloy bone screw before implantation.

residual implants decreased. Micro-computed tomographic reconstruction image of the same specimen displayed similar characteristics. Superb direct bone deposition and new bone formation around the partly absorbed Mg-5 wt%Ca-1 wt%Zn alloy bone screw was observed after 24 weeks of implantation as shown in Fig. 5. There was no adverse effect from the implant material and controlled slow corrosion rate of the alloy allowed the developed bone screw to remain in the implantation site while promoting direct new bone deposition and growth. New orthopedic implant made out of extruded Mg-5 wt%Ca-1 wt%Zn alloy will be slowly absorbed by the physiological surroundings while maintaining its mechanical integrity over the implantation period until being completely replaced with the new bone.

Discussion

We identified a biodegradable Mg implant material that can reduce or control hydrogen evolution remarkably during *in vitro* and *in vivo* degradation. This effect was achieved by both microstructural and electrochemical tailoring; specifically, via a modified microstructure produced by mechanical extrusion and an increase in OCP of Mg_2Ca induced by dissolved Zn. The large reduction in hydrogen evolution to levels comparable to those of previous glassy Mg alloys[22] reported represents a significant step toward the use of Mg in biodegradable implants in this study for the first time. The further adequate tissue healing seen in conjunction with these alloys and their good mechanical properties indicate that the extruded Mg-5 wt%Ca-*x*wt%Zn ($1 \leq x \leq 3$) alloys investigated are ideal candidates for biodegradable implant applications.

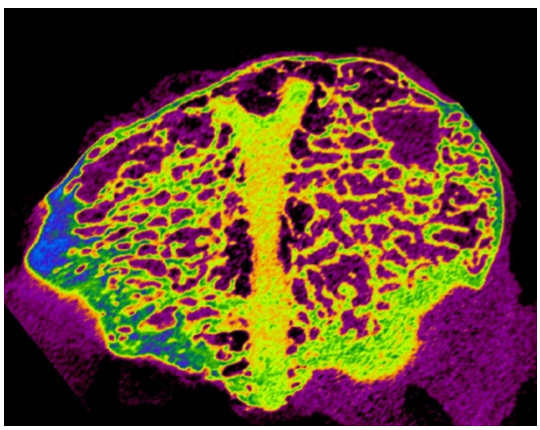

Figure 5 | Micro-computed tomographic image of extruded Mg-5 wt%Ca-1 wt%Zn alloy bone screw in femoral condyle at 24 weeks after operation.

Methods

Preparation of Mg alloys. Air and moisture in the furnace were removed by evacuating up to 5×10^{-2} torr at room temperature before Ar gas was allowed to flow into the furnace. Commercial pure Mg (99.98%) ingots, Ca (99.6%) metal grains, and Zn (99.99%) metal grains were melted in a stainless steel crucible under an Ar atmosphere at 790°C for 120 min, after which the molten alloy was stirred for 5 min. Subsequently, the alloy was poured into a stainless steel mold that had been preheated to 500°C and then cooled in the furnace. The chemical compositions of the samples were determined by inductively coupled plasma (ICP, ARIAN 710-ES) analysis.

Mechanical extrusion. For direct extrusion with an extrusion ratio of 25 : 1, the as-cast Mg alloys were machined as a billet 50 mm in diameter and 60 mm in length. The billet was preheated to 350°C and then placed in a container heated to 350°C, after which it was extruded at a ram speed of 0.2 mm/s. The exit temperature was maintained at 250°C.

Immersion tests. Each sample used for the immersion test was machined to six plates ($20 \times 10 \times 1.5$ mm^3), after which all of the surfaces were ground with SiC papers with up to 2000 grit. Each sample plate was immersed in Hank's solution with a pH of 7.4, which was controlled by HCl and NaOH and the pH was then allowed to change during the immersion test. The hydrogen evolution caused the water surface to descend with time in a funnel system. The amount of hydrogen evolution was measured by checking the variation in the height of the water surface with time.

SEM observation. After the immersion test, the corroded samples were mounted using a mixture of resin and hardener. After hardening, the specimens were polished using 0.25 μm diamond powder and anhydrous ethanol (99.98%). The microstructures of the corroded samples were then observed by electron probe micro analyzer (JEOL JXA-8500F).

OCP measurement. To understand the biodegradation behavior of each phase in the Mg-Ca-Zn alloy, the OCP of pure Mg (99.98%), Mg_2Ca, and Mg_2Ca(Zn) was measured using the Autolab-GPES Version 4.8 corrosion measurement system. The sample preparation was the same as for the fabrication of Mg alloys described above and Mg_2Ca samples with Zn were fabricated from Mg_2Ca ingot custom-made from R&D Korea. The chemical compositions of the samples were then determined by inductively coupled plasma (ICP, ARIAN 710-ES) analysis.

Work function calculation. Density functional theory (DFT) calculations using the VASP program packages[34] were used. The plane wave basis expansions with an energy cutoff of 300 eV and the generalized gradient approximation (GGA) with the PW91 exchange-correlation functional were used. The core-valence interaction is described by the projector-augmented wave (PAW) method[35]. We constructed Mg_2Ca slab structure with 96 Mg atoms and 48 Ca atoms to calculate work function. Vacuum sizes were given larger than 20 Å to minimize interaction between slabs. We first obtained the bulk Mg_2Ca structure applying Monkhorst-Pack sampling with a $8 \times 8 \times 4$ k-point grid and then constructed a slab structure with the resulting lattice constant and a $3 \times 3 \times 1$ k-point grid.

WDS analysis. The two-dimensional distribution of the Zn composition shown in Fig. 2 was obtained by WDS analysis (JEOL JXA-8500F). The sample preparation was the same as that used for SEM analysis.

Radiographic analysis. Upon approval from the Animal Care and Use Committee of Chungnam National University, *in vivo* hydrogen evolution caused by the corrosion of newly developed magnesium alloys was investigated using eight adult male Sprague-Dawley rats weighing approximately 400 g (Orient Bio, Gyunggi, South Korea). Rats were anesthetized with 0.8 ml ketamine with 0.01 ml lumpun. Four types of 1 mm thick, 5 mm wide, and 20 mm long plates (cast and extruded Mg-5 wt%Ca and Mg-5 wt%Ca-1 wt%Zn alloys) were implanted into the dorsal abdominal region. Daily observations were made and radiographic examinations of gas pockets were conducted at weeks 4 and 12.

Histological analysis. The *in vivo* evaluations including histological analysis and micro-computed tomographic analysis were performed at AccelLab (Quebec, Canada) in compliance with 21 CFR part 58 (FDA) Good Laboratory Practice for Nonclinical Laboratory Studies. Histological analysis was carried out to investigate the performance of the newly developed biodegradable Mg alloy screw of 2 mm in outer diameter and of 10 mm in length *in vivo* for 24 weeks. Twenty-one New Zealand white rabbits were assigned for this study and all animals received a bilateral implantation of Mg alloy screw in the femoral condyle. Animals were sacrificed at 24 weeks after the operation and the distal portions of the femurs containing the implantation sites were harvested and fixed in 100% ethanol. The bone blocks comprising the implant sites were processed, infiltrated with Technovit 7200, and polymerized. After embedding, the blocks were cut adjacent to the implant material by sawing along the longitudinal axis of the sample and sections were stained with Toludine blue.

Micro-computed tomographic analysis. Bone blocks from histological study comprising implant units and surrounding bone were scanned using Skyscan Micro CT equipment. Images were used to reconstruct a 3-D image of the implant unit and the long axis of the implant was aligned perpendicularly to the axis of the X-ray beam.

1. Park, J. B. & Bronzino, J. D. *Biomaterials: Principles and Applications.* (Taylor & Francis, 2002).
2. Saris, N. E., Mervaala, E., Karppanen, H., Khawaja, J. A. & Lewenstam, A. Magnesium. An update on physiological, clinical and analytical aspects. *Clinica chimica acta; international journal of clinical chemistry* **294**, 1–26 (2000).
3. Ducheyne, P. & Hastings, G. W. *Functional Behavior of Orthopedic Biomaterials: Applications.* (CRC Press, 1984).
4. Davis, J. R. *Handbook of materials for medical devices.* (ASM international, 2003).
5. Zhang, E., Xu, L. & Yang, K. Formation by ion plating of Ti-coating on pure Mg for biomedical applications. *Scripta Materialia* **53**, 523–527 (2005).
6. Revell, P. A., Damien, E., Zhang, X., Evans, P. & Howlett, C. R. The effect of magnesium ions on bone bonding to hydroxyapatite coating on titanium alloy implants. *Key Engineering Materials* **254**, 447–450 (2004).
7. Zreiqat, H. *et al.* Mechanisms of magnesium-stimulated adhesion of osteoblastic cells to commonly used orthopaedic implants. *Journal of biomedical materials research* **62**, 175–184 (2002).
8. Yamasaki, Y. *et al.* Synthesis of functionally graded MgCO3 apatite accelerating osteoblast adhesion. *Journal of biomedical materials research* **62**, 99–105 (2002).
9. Yamasaki, Y. *et al.* Action of $FGMgCO_3$ Ap-collagen composite in promoting bone formation. *Biomaterials* **24**, 4913–4920 (2003).
10. Li, Z., Gu, X., Lou, S. & Zheng, Y. The development of binary Mg–Ca alloys for use as biodegradable materials within bone. *Biomaterials* **29**, 1329–1344 (2008).
11. Witte, F. *et al.* In vivo corrosion of four magnesium alloys and the associated bone response. *Biomaterials* **26**, 3557–3563 (2005).
12. Wen, C. *et al.* Processing of biocompatible porous Ti and Mg. *Scripta Materialia* **45**, 1147–1153 (2001).
13. Hofmann, G. Biodegradable implants in traumatology: a review on the state-of-the-art. *Archives of orthopaedic and trauma surgery* **114**, 123–132 (1995).
14. Vormann, J. Magnesium: nutrition and metabolism. *Molecular aspects of medicine* **24**, 27–37 (2003).
15. Atrens, A., Liu, M. & Zainal Abidin, N. I. Corrosion mechanism applicable to biodegradable magnesium implants. *Materials Science and Engineering: B* **176**, 1609–1636 (2011).
16. Staiger, M. P., Pietak, A. M., Huadmai, J. & Dias, G. Magnesium and its alloys as orthopedic biomaterials: a review. *Biomaterials* **27**, 1728–1734 (2006).
17. Song, G. Control of biodegradation of biocompatable magnesium alloys. *Corrosion Science* **49**, 1696–1701 (2007).
18. Gu, X., Zheng, Y., Cheng, Y., Zhong, S. & Xi, T. In vitro corrosion and biocompatibility of binary magnesium alloys. *Biomaterials* **30**, 484–498 (2009).
19. Lambotte, A. L'utilisation du magnesium comme materiel perdudansl'osteosynthè se. *Bull MémSoc Nat Chir* **28**, 1325–1334 (1932).
20. Troitskii, V. & Tsitrin, D. The resorbing metallic alloy 'Osteosinthezit' as material for fastening broken bone. *Khirurgiia* **8**, 41–44 (1944).
21. Zhang, S. *et al.* Research on an Mg–Zn alloy as a degradable biomaterial. *Acta Biomaterialia* **6**, 626–640 (2010).
22. Zberg, B., Uggowitzer, P. J. & Löffler, J. F. MgZnCa glasses without clinically observable hydrogen evolution for biodegradable implants. *Nature Materials* **8**, 887–891 (2009).
23. Jacobs, J. J., Hallab, N. J., Skipor, A. K. & Urban, R. M. Metal degradation products: a cause for concern in metal-metal bearings? *Clinical orthopaedics and related research* **417**, 139–147 (2003).
24. Niki, Y. *et al.* Metal ions induce bone-resorbing cytokine production through the redox pathway in synoviocytes and bone marrow macrophages. *Biomaterials* **24**, 1447–1457 (2003).
25. Ma, E. & Xu, J. Biodegradable alloys: the glass window of opportunities. *Nature Materials* **8**, 855–857 (2009).
26. Gu, X. *et al.* Corrosion of, and cellular responses to Mg–Zn–Ca bulk metallic glasses. *Biomaterials* **31**, 1093–1103 (2010).
27. Witte, F. *et al.* Degradable biomaterials based on magnesium corrosion. *Current Opinion in Solid State and Materials Science* **12**, 63–72 (2008).
28. Isabel Post, J., Karl Eibl, J. & Michiel Ross, G. Zinc induces motor neuron death via a selective inhibition of brain-derived neurotrophic factor activity. *Amyotrophic Lateral Sclerosis* **9**, 149–155 (2008).
29. Rad, B. *et al.* Characterization and corrosion behavior of biodegradable Mg-Ca and Mg-Ca-Zn implant alloys. *Applied Mechanics and Materials* **121**, 568–572 (2012).
30. Du, H., Wei, Z., Liu, X. & Zhang, E. Effects of Zn on the microstructure, mechanical property and bio-corrosion property of Mg–3Ca alloys for biomedical application. *Materials Chemistry and Physics* **125**, 568–575 (2011).
31. Zhang, E. & Yang, L. Microstructure, mechanical properties and bio-corrosion properties of Mg–Zn–Mn–Ca alloy for biomedical application. *Materials Science and Engineering: A* **497**, 111–118 (2008).
32. Ralston, K. & Birbilis, N. Effect of grain size on corrosion: a review. *Corrosion* **66**, 075005-075005–075013 (2010).
33. Yee, S., Oriani, R. & Stratmann, M. Application of a Kelvin microprobe to the corrosion of metals in humid atmospheres. *Journal of the Electrochemical Society* **138**, 55–61 (1991).
34. Kresse, G. & Furthmüller, J. Efficiency of ab-initio total energy calculations for metals and semiconductors using a plane-wave basis set. *Computational Materials Science* **6**, 15–50 (1996).
35. Blöchl, P. E. Projector augmented-wave method. *Physical Review B* **50**, 17953 (1994).

Acknowledgements

This study was supported by the KIST Project (2E23720) and Seoul R&BD program, Seoul Development Institute, Republic of Korea (SS100008). PRC acknowledges the supports by Priority Research Centers Program through the National Research Foundation of Korea (NRF) funded by the Ministry of Education, Science and Technology (2010-0028287), by the Korea Science and Engineering Foundation (KOSEF) grant funded by the Korea government (MEST) (No. R11-2005-048-00000-0) and by Basic Science Research Program through the National Research Foundation of Korea (NRF) funded by the Ministry of Education, Science and Technology (2012R1A1A2006933).

Author contributions

P.-R.C., H.-S.H., G.-F.Y., Y.-Y.K., K.-S.L. and Y.-C.K. were responsible for the preparation of samples and testing of their mechanical properties and in vivo behaviors. P.-R.C. designed and performed series of simulation required to engineer the alloys with K.-H.H. and S.-C.L. J.-Y.J., J.-Y.B. and J.-P.A. performed imaging analysis. S.-Y.C., S.-J.Y. and H.-K.S. designed the research and supervised the project. All authors contributed to the writing of the paper and take full responsibility for the content.

Additional information

Supplementary information accompanies this paper at http://www.nature.com/scientificreports

Competing financial interests: The authors declare no competing financial interests.

How to cite this article: Cha, P.-R. *et al.* Biodegradability engineering of biodegradable Mg alloys: Tailoring the electrochemical properties and microstructure of constituent phases. *Sci. Rep.* **3**, 2367; DOI:10.1038/srep02367 (2013).